Control of frequency chirp in nanosecond-pulsed laser spectroscopy. 3. Spectrotemporal dynamics of an injection-seeded optical parametric oscillator

Richard T. White,[1,4] Yabai He,[2] Brian J. Orr,[2,*] Mitsuhiko Kono,[3] and K. G. H. Baldwin[3]

[1]*Industrial Research Ltd., P. O. Box 31–310, Lower Hutt, New Zealand*
[2]*Centre for Lasers and Applications, Macquarie University, Sydney, New South Wales 2109, Australia*
[3]*Research School of Physical Sciences and Engineering, Australian National University, Canberra, Australian Capital Territory 0200, Australia*
[4]*Current address: Ministry of Research, Science and Technology, P. O. Box 5336, Wellington 6145, New Zealand*
[*]*Corresponding author: borr@ics.mq.edu.au*

Received March 16, 2007; revised July 25, 2007; accepted July 26, 2007;
posted August 2, 2007 (Doc. ID 81084); published September 17, 2007

Complicated spectrotemporal processes are associated with the generation of signal and idler output pulses on a nanosecond timescale in an injection-seeded optical parametric oscillator (OPO). The mechanisms of such spectrotemporal dynamics are revealed by numerical simulation, including innovative modeling of instantaneous-frequency profiles and frequency chirp. These simulations are in satisfactory agreement with optical-heterodyne measurements of output from a nanosecond-pulsed OPO system that is based on periodically poled $KTiOPO_4$, pumped at 532 nm by a Nd:YAG laser and injection-seeded at a signal wavelength of ~842 nm. Frequency chirp in narrowband signal output pulses from such an OPO system has previously been observed to depend on phase mismatch between the pump, signal, and idler waves, and also on the pump-pulse energy. Our simulations accurately predict this behavior and yield realistic estimates of the frequency chirp, optical bandwidth, and spectral purity of the signal output pulse as it evolves, including effects that are not readily observed directly. This approach provides insight into instrumental conditions that facilitate continuously tunable, single-longitudinal-mode operation of such a pulsed OPO system, with optical bandwidth as close as possible to the Fourier-transform limit.

OCIS codes: 070.4790, 120.5050, 190.4410, 190.4970.

1. INTRODUCTION

Pulsed optical parametric oscillators (OPOs) operating on nanosecond time scales are useful coherent light sources for applications requiring broad wavelength tunability and/or access to wavelength regions in which there are no suitable lasers. However, it is likely that nanosecond-pulsed OPOs have not yet reached their full potential in many applications. This may be attributed to several factors, particularly the requirement for high-quality pump lasers, ease of optical damage to the nonlinear-optical (NLO) medium, and the complicated and often unwanted behavior associated with the NLO interaction. Recently, there has been renewed fundamental interest in the temporal, spatial, and spectral performance of nanosecond-pulsed OPOs, within our own group [1–4] and elsewhere [5–9]. Effects such as frequency chirp, the breakdown of seeding during signal and idler pulse generation, reduced backconversion, spatial beam quality, spatiotemporal dynamics, and spectrotemporal dynamics have been measured and modeled under various operating conditions, for both birefringently phase-matched and quasi-phase-matched (QPM) NLO media. Numerical simulation studies of such processes, in and beyond the range in which they are observed, offer insight into mechanisms that are at work in injection-seeded nanosecond-pulsed OPOs and thereby enable their design and performance to be improved.

For example, we have used an optical-heterodyne (OH) technique [2] to measure temporal characteristics of the optical frequency of output pulses from a nanosecond-pulsed injection-seeded OPO system [1,3], using periodically poled $KTiOPO_4$ (PPKTP) in a cavity that is resonant at the (seeded) signal wavelength. This system exhibits single-longitudinal-mode (SLM) operation, with frequency chirp that is minimal when the phase mismatch (Δk) is close to zero. Also, under certain conditions (excessive pump-pulse energy and/or Δk), seeding is found to fail partway through the output pulse, such that operation on multiple longitudinal modes ensues [3,4]. Incidentally, our ability to monitor frequency chirp and pulse-to-pulse fluctuations in the central frequency of the SLM output from such an OPO system has resulted in a new form of sub-Doppler spectroscopy: coherent heterodyne-assisted pulsed spectroscopy (CHAPS) [10,11].

This paper is the third in a series [2,3] on characterization of the instantaneous frequency of output from our high-performance pulsed OPO system, based on a QPM NLO medium [3,4,10–12]. Here we present new tempo-

rally resolved computer simulations of the spectroscopic performance of this OPO system. The simulated outcomes are compared with experimental results, as a constructive adjunct to our previous investigations [1–4]. This paper is also effectively a continuation and extension of earlier OPO simulation studies by other researchers, notably Arisholm *et al.* [5] and Smith [9].

Our simulations confirm and help to explain various forms of spectrotemporal dynamics (e.g., the transition from SLM to multimode operation during a signal or idler output pulse) that are observed in such an OPO system. The simulations provide insight into operating conditions that facilitate continuously tunable, SLM operation of the OPO, with optical bandwidth as close as possible to the Fourier-transform (FT) limit. We note that numerical simulation of OPO operation is not only complementary to experimental measurements, but also supplementary in that the former can access operating conditions and performance characteristics that are not readily accessible to the latter.

2. INSTRUMENTATION

Design details of our OPO system have been presented elsewhere [1,3]. The oscillator itself comprises a QPM NLO crystal (PPKTP, 20 mm long with a 9.35 μm grating period) in a bow-tie ring resonator (114 mm long) that is locked to the wavelength of a narrowband (typically $<$1 MHz FWHM) continuous-wave (cw) injection seeder. Two of the four cavity mirrors are 80% reflective at the signal wavelength, whereas the other two mirrors are highly reflective ($>$99%). The OPO is singly resonant at the signal wavelength and, in the absence of seeding, yields a free-running signal output wavelength λ_{free} $=841.75\pm0.01$ nm for a crystal temperature of 125°C. In the present context, the injection seeder is an external-cavity diode laser with a typical tuning range of 834–851 nm. It has already been demonstrated [3] that minimal frequency chirp is attainable when the wavelength λ_s of the injection seeder equals the free-running phase-matched wavelength λ_{free}, i.e., when $\lambda_s=\lambda_{free}$. The pump source is a 532 nm SLM Nd:YAG laser with long pulse duration (~27 ns, FWHM). The OPO generates pulses of signal and idler output radiation with nearly FT-limited optical bandwidth. The ~10 μJ signal pulses can be amplified by a birefringently phase-matched $LiNbO_3$ optical parametric amplifier, pumped by the same Nd:YAG laser. An OH detection system and a FT analysis technique [2,3] allow us to record the instantaneous optical frequency profile, $f_{inst}(t)$, of each pulse, thereby facilitating spectroscopic measurements that require low frequency chirp (e.g., as in our recent CHAPS studies [10,11]). Figure 1 shows a computer screen dump of the front end of the interactive real-time FT chirp analysis software that we have developed for experimental convenience since our earlier papers [1–3].

The top left-hand panel depicts an experimentally recorded waveform of OH beats between a single OPO signal pulse and the cw seed radiation that has been frequency-shifted by an acousto-optic modulator (AOM). This beat waveform contains all of the instantaneous-

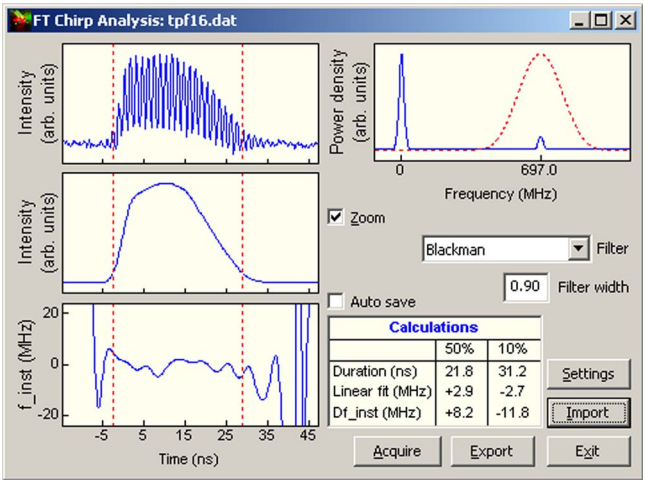

Fig. 1. (Color online) Computer screen dump of recently developed interactive software for chirp analysis, based on optical-heterodyne detection and a Fourier-transform algorithm. The software displays, in real time, the recorded beat waveform (top, left) and its Fourier transform (with filter function; top and center, right), the reconstructed OPO signal pulse profile (center, left), the calculated $f_{inst}(t)$ profile (bottom, left), and a summary of calculated pulse durations and chirp parameters (bottom right) for 50% and 10% intensity ranges. Vertical dashed lines in the left-hand panels designate the 10% intensity points. In this example, the OPO is well seeded and the frequency chirp is very low ($<$10 MHz).

frequency and chirp information to be extracted for that particular OPO signal pulse.

The top right-hand panel of Fig. 1 displays the Fourier transform of the beat waveform, with superimposed sideband filter function (e.g., Blackman or Tukey types) [2,12–16] as specified in the central right-hand section below that panel, centered at 697.0 MHz (corresponding to the peak of the sideband). The central and bottom left-hand panels of Fig. 1 show results of Fourier back-transformation: the reconstructed OPO signal pulse profile and the calculated $f_{inst}(t)$ profile, respectively. Vertical dashed lines in the three left-hand panels designate 10% intensity points, while the table in the bottom right-hand section of Fig. 1 summarizes calculated pulse durations and chirp parameters (Δf_{inst} and straightline fit) [2,3] for the 50% and 10% intensity intervals.

In regular operation, the FT chirp-analysis software acquires data from the digital oscilloscope (e.g., Tektronix model TDS3054B, in this case) or other recording system. It then displays the outcome of real-time FT and filtering processes, exports data for subsequent processing, and awaits the next OPO shot. In the particular example illustrated in Fig. 1, the injection-seeding conditions for the OPO have been selected such that the frequency chirp is very low: $<$10 MHz, as estimated by either Δf_{inst} or straight-line fit methods within the 50% intensity range of 21.8 ns.

3. NUMERICAL SIMULATION

The SNLO nonlinear optics code of Smith [17] has proved to be an extremely useful tool in performing the numeri-

cal simulations reported in this paper. We have made use of two plane-wave (PW) models that are available within the SNLO software package [17], namely:

- PW-OPO-LP, a monochromatic model that ignores group-velocity differences between the pump, signal, and idler waves and is suitable for modeling narrowband nanosecond or longer pulses (or cw output); and
- PW-OPO-BB, a broadband (BB) model that accounts for group-velocity differences and is able to simulate BB OPO operation (e.g., unseeded or partially seeded).

These models do not include an explicit frequency dependence of the pump, signal, and idler waves. Spectral information is obtained by Fourier analysis of the complex-valued time-dependent field amplitudes. The SNLO models provide fresh information that helps us to optimize narrowband operation of our nanosecond-pulsed PPKTP OPO system. As in other recent studies [5,8,9,18], we do not attempt in the present investigation to simulate spatial beam quality [6] or spatiotemporal dynamics [7]. The 2D-OPO-LP feature of SNLO, based on monochromatic waves with transverse Gaussian spatial structure, is therefore not needed in this paper. Table 1 shows relevant adjustable parameters that have been used as input to the SNLO model.

Previous studies of BB models with and without transverse structure have shown that the PW approach is a satisfactory way to model optical-phase effects (such as optical bandwidth) [5,9]. The computational complexity of the detailed analysis presented in this paper precludes simultaneous modeling of optical bandwidth and transverse beam structure.

In a related context, Anstett and Wallenstein [8] have measured spectrotemporal dynamics in a short-cavity pulsed OPO, and discussed their results in terms of the classic simulations of Cassedy and Jain [19]. In Subsections 3.A, 3.B, and 3.C we consider specific results that entail a comparison of our previously reported measurements [1,3,4,10,11] with our more recent simulations.

A. Temporal Profiles of Depleted Pump and Signal Output Pulses

In the following comparison of observed and simulated results, the PPKTP OPO is usually (unless noted otherwise) operated with the free-running signal output wavelength λ_{free} maintained at 841.75 ± 0.01 nm and, if injection-seeded, with the seeded signal wavelength λ_s set equal to λ_{free} (i.e., under seeding conditions that minimize frequency chirp [3]). The threshold of pump pulse energy E_p for unseeded (free running) operation in these experiments is $\sim 27\ \mu$J; this provides a useful reference point for "times-above-threshold" comparisons between similar OPOs operating with different pump-pulse thresholds. As in earlier work [3,4], we use a parameter R_p defined as the ratio between the actual value of E_p and the threshold pump-pulse energy for the *unseeded* OPO.

Observed (○) and calculated (dashed curve) signal output pulse energies from the PPKTP OPO seeded at $\lambda_s = 841.78$ nm are plotted in Fig. 2, with pump-pulse energy E_p ranging from the threshold for seeded operation ($\sim 19\ \mu$J; $R_p \approx 0.7$) to $108\ \mu$J ($R_p \approx 4$). The simulations, based on the PW-OPO-LP model [17], agree satisfactorily with experiment within this range. Figure 2 also shows corresponding results for the unseeded (free running) PPKTP OPO. Signal output pulse energies, observed (×) and simulated by PW-OPO-LP (solid curve), display a significantly higher threshold ($\sim 27\ \mu$J; $R_p = 1.0$) relative to that of the seeded OPO, bearing out expectations [19] that injection seeding will effectively lower the threshold for a particular mode of the OPO cavity. However, unseeded signal output pulse energies are in poor agreement when E_p exceeds $\sim 70\ \mu$J($R_p \approx 2.6$): a discrepancy addressed and resolved in our subsequent simulations.

The vertical arrows in Fig. 2 designate the three values of E_p for which simulated temporal profiles of depleted pump and signal output pulses are presented in Fig. 3. The temporal profiles displayed in Fig. 3 have been simulated by the SNLO PW-OPO-LP model for the following E_p and R_p values: (a) and (b) $E_p = 30\ \mu$J, $R_p \approx 1.1$; (c) and

Table 1. Adjustable Parameters Used as Input to the SNLO Model

Adjustable Model Parameters	Value(s)		
Length of four-mirror OPO ring cavity (mm)	114		
Length of PPKTP crystal (mm)	20		
Phase mismatch range, Δk (cm^{-1}), for PPKTP	−0.823 to 1.05		
Effective nonlinear-optical coefficient, d_{eff} ($pm\,V^{-1}$), for PPKTP	9.74		
Wavelength-dependent Quantities	Pump	Signal	Idler
Wavelength (nm)	532	842	1445
Refractive index for PPKTP	1.891	1.843	1.820
Group-velocity index for PPKTP	2.066	1.904	1.855
Input pulse energy range (μJ)	0–108	0	0
Input pulse duration (ns, FWHM)	25	0	0
Beam diameter (mm, FWHM)	0.350	0.175	0.175
Input cw seed power (mW)	—	1 (seeded) or 0 (unseeded)	0
Input-mirror reflectivity (%)	3	80	0
Output-mirror reflectivity (%)	0	80	0

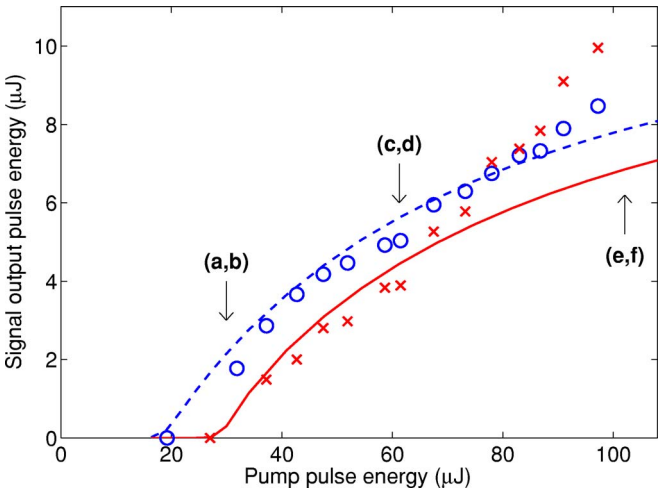

Fig. 2. (Color online) Monochromatic plane-wave simulations, based on the SNLO PW-OPO-LP code [17], of signal output pulse energies as a function of pump pulse energy E_p for a pulsed PPKTP OPO that is operated *either* unseeded and free running (solid curve) with $\lambda_{free}=841.75\pm0.01$ nm *or* injection seeded (dashed curve) with $\lambda_s=841.76$ nm (i.e., effectively equal to λ_{free}, to minimize frequency chirp). Corresponding observed signal output pulse energies [3] are also plotted (×=unseeded, free running; ○=injection seeded). Vertical arrows designate the three values of pump pulse energy E_p for which simulated temporal profiles are presented in Fig. 3.

(d) $E_p=61\,\mu$J, $R_p\approx2.2$; and (e) and (f) $E_p=102\,\mu$J, $R_p\approx3.8$. Dashed and solid curves correspond to the seeded and unseeded OPO, respectively. The left-hand panels show the input pump pulses (dotted–dashed curves, Gaussian, 25 ns FWHM) in addition to the two forms of depleted pump pulse. The corresponding temporal profiles for signal output pulses are shown in the right-hand panels. As expected [19], the onset of the signal output pulse and the associated pump-depletion dip occur significantly earlier for the seeded OPO than for the unseeded OPO. Likewise, these onsets occur at markedly earlier times as E_p increases from just above the threshold for unseeded OPO operation in Figs. 3(a) and 3(b) to almost four times that threshold in Figs. 3(e) and 3(f).

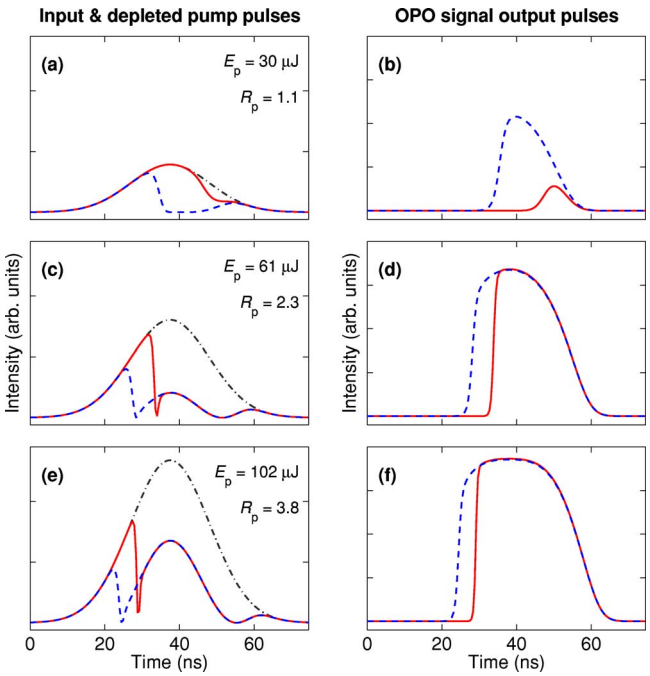

Fig. 3. (Color online) SNLO PW-OPO-LP simulations [17] of PPKTP OPO temporal profiles (solid curves, unseeded, free running; dashed curves, injection seeded) for depleted pump pulses (left-hand column) and signal output pulses (right-hand column), at the three arrowed settings of E_p in Fig. 2. Input pump pulse profiles are depicted by dotted–dashed curves in the left-hand column.

The signal and depleted-pump profiles presented in Fig. 3, and also in Fig. 4, provide clear indications of backconversion from the signal and idler waves to the pump, together with the associated clamping of signal and idler intensities. Such behavior becomes more pronounced as E_p increases. It has been found [5,9,18] that backconversion is maximized when the group-velocity index of the pump wave ($n_{g,p}$) is midway between those of the signal

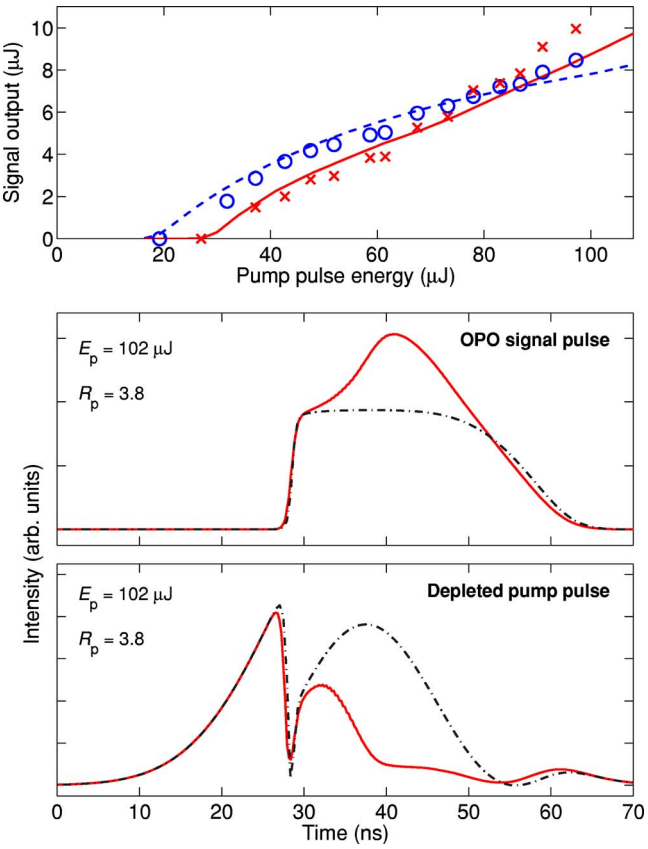

Fig. 4. (Color online) Top: broadband PW simulations, based on the SNLO PW-OPO-BB code [17], of signal output pulse energies as a function of pump pulse energy E_p for a pulsed PPKTP OPO that is operated *either* unseeded and free running (solid curve) *or* injection seeded (dashed curve) with corresponding observed signal output pulse energies [3] (×=unseeded, free running; ○=injection seeded) as in Fig. 2. Center: PW-OPO-BB simulation (solid curve) of the temporal profile for the signal output pulse from the unseeded PPKTP OPO with $E_p=102\,\mu$J and $R_p=3.8$. The corresponding PW-OPO-LP simulation is shown for comparison (dotted-dashed curve). Bottom: corresponding PW-OPO-BB (solid curve) and PW-OPO-LP (dotted–dashed curve) simulations of the temporal profile for the depleted pump pulse from the unseeded PPKTP OPO. The PW-OPO-BB simulations provide a more realistic representation of the unseeded OPO because backconversion effects are more adequately treated by the PW-OPO-BB model than by the PW-OPO-LP model.

and idler waves ($n_{g,s}$ and $n_{g,i}$, respectively). This also minimizes amplitude modulation of the three waves, thereby reducing the tendency to BB operation.

As already remarked, the PW-OPO-LP predictions shown in Fig. 2 agree well with the experimental results for most of the range of pump-pulse energies E_p that we have explored. We do not expect perfect agreement partly because the PW approximation of the SNLO models does not accurately match the approximately Gaussian transverse profile of the beams in our OPO. Above $E_p \approx 70\ \mu J$ ($R_p \approx 2.6$) the PW-OPO-LP curve in Fig. 2 significantly underestimates the output signal pulse energy in the case of unseeded operation. Much better agreement between the observed ($\times$) and simulated (solid curve) signal output pulse energies is obtained when we use the SNLO PW-OPO-BB model, as shown in the top section of Fig. 4. This improvement is attributable to the fact that the monochromatic PW-OPO-LP model ignores group-velocity differences between the pump, signal, and idler waves, whereas the PW-OPO-BB model is able to simulate unseeded or partially seeded OPO operation.

In the case of the PW-OPO-BB simulation with $E_p = 102\ \mu J$ ($R_p \approx 3.8$), the center and bottom sections of Fig. 4 (solid curves) show, respectively, that the conversion efficiency is increased and is accompanied by reduced backconversion, relative to a PW-OPO-LP simulation (shown as dotted–dashed curves). In addition, signal–idler walk-off (which we estimate to be ~3 ps) gives rise to rapid oscillations in the signal and idler field amplitudes. However, these oscillations cannot be detected by our OH detection system (which has a 1 GHz bandwidth); they are therefore not shown in Fig. 4; see Subsection 3.C for more information.

Behavior shown in Fig. 4 (as well as the unobserved fast oscillations) is consistent with the fact that OPO efficiency and optical bandwidth increase significantly if the group velocity $n_{g,p}$ differs substantially from $n_{g,s}$ and $n_{g,i}$ [5,9,18]. From Sellmeier and thermo-optic dispersion formulas [20], we estimate that the group-velocity index of the pump wave (at $\lambda_p = 532$ nm) in our OPO is $n_{g,p} = 2.066$: far from those of the signal ($\lambda_s \approx 842$ nm; $n_{g,s} = 1.904$) and the idler ($\lambda_i \approx 1445$ nm; $n_{g,s} = 1.855$) waves. Our calculations of seeded operation show that the onset of this reduction in backconversion occurs just beyond the upper limit of the abscissa (i.e., above $E_p = 108\ \mu J$ and $R_p \approx 4$). Effects of this type are discussed in more detail in Subsection 4.C.

B. Frequency Chirp in the Signal Output

It is understood from previous work [1,3,21,22] that the magnitude and sign of frequency chirp in the output signal pulses depend on several factors, particularly phase mismatch Δk, detuning of the seed frequency from the OPO cavity-resonance frequency, and pump-pulse energy E_p. We have found [1,3] that the most effective way to minimize (or control) the frequency chirp is via Δk. This is illustrated in Fig. 5, where profiles of the instantaneous frequency $f_{inst}(t)$ are simulated (for the first time, as far as we know) by the SNLO PW-OPO-LP model for signal output pulses over a range of values of Δk, from −0.823 to 1.05 cm^{-1}. This Δk range can be accessed experimentally by varying the seed wavelength between 841.5 and 842 nm [3].

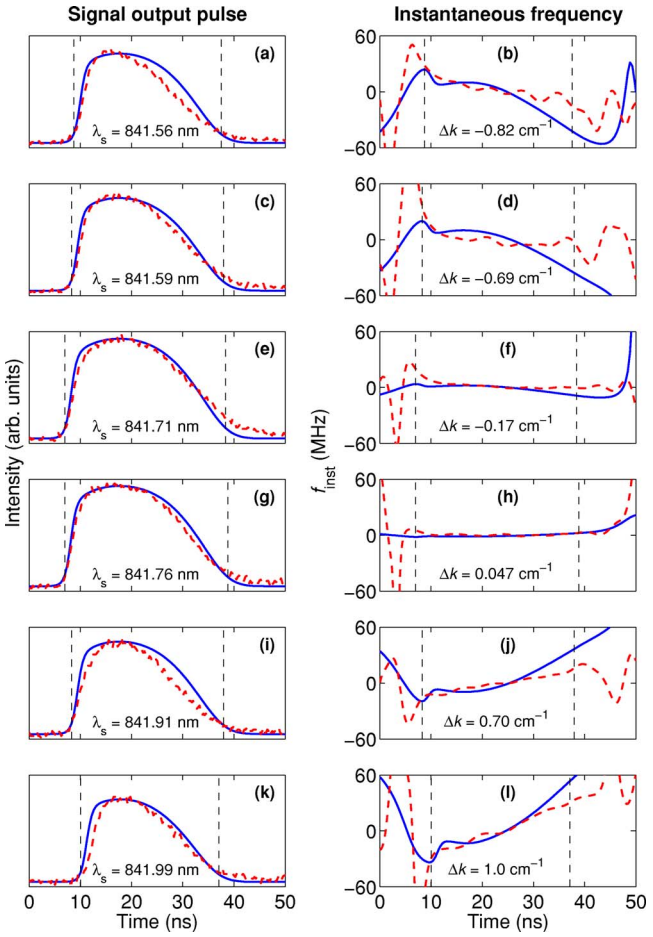

Fig. 5. (Color online) SNLO PW-OPO-LP simulations [17] of PPKTP OPO operation with $R_p = 2$, for a variety of detunings of seeded signal wavelength λ_s from λ_{free} and corresponding phase mismatches Δk. The left-hand column shows measured (dashed curve) and simulated (solid curve) temporal profiles of the OPO signal output pulse, with λ_s values annotated. The right-hand column shows experimental (dashed curves) and simulated (solid curves) profiles of the instantaneous frequency $f_{inst}(t)$, with Δk values annotated. These results confirm our previous observations [1,3] that the frequency chirp is approximately proportional to Δk and that it is minimized by setting $\Delta k = 0$.

The simulations presented in Fig. 5 correspond to the six sets of measurements of $f_{inst}(t)$ that were previously reported in Fig. 4 of [3], for the following six pairs of s and Δk, relative to $\lambda_{free} = 841.75$ nm: (a) and (b) $\lambda_s = 841.56$ nm, $\Delta k = -0.823$ cm^{-1}; (c) and (d) $\lambda_s = 841.59$ nm, $\Delta k = -0.692$ cm^{-1}; (e) and (f) $\lambda_s = 841.71$ nm, $\Delta k = -0.171$ cm^{-1}; (g) and (h) $\lambda_s = 841.76$ nm, $\Delta k = 0.047$ cm^{-1}; (i) and (j) $\lambda_s = 841.91$ nm, $\Delta k = 0.698$ cm^{-1}; (k) and (l) $\lambda_s = 841.99$ nm, $\Delta k = 1.045$ cm^{-1}. Note that, for traces (g) and (h) where $\Delta k \approx 0$, λ_s is effectively set equal to λ_{free} (within the ±0.01 nm tolerance of our pulsed wavemeter for a free-running OPO).

The results in Fig. 5 correspond to a pump level of $R_p = 2$ (i.e., twice the threshold of the unseeded free-running PPKTP OPO: a typical operating level). The left-hand column of Fig. 5 shows measured and simulated temporal

profiles of the OPO signal output pulse, at each of the six values of λ_s and Δk. Experimental and simulated $f_{inst}(t)$ profiles, plotted the right-hand column of Fig. 5 as dashed and solid curves, respectively, agree well and confirm our previous observations [1,3] that the frequency chirp is approximately proportional to Δk and that it can be minimized by arranging for the phase mismatch Δk to be zero (e.g., by adjusting the temperature of the QPM crystal).

From the numerical simulations, this peak (or "central" [10,11]) frequency is found to depend on Δk: $f_{peak}=f_{carrier}+m_{sim}\Delta k$, where $f_{carrier}$ is the constant optical carrier frequency in the slowly varying envelope approximation [18] and $m_{sim}\approx -82.2\pm 0.2$ MHz cm. The corresponding effect in our experimental $f_{inst}(t)$ data [3] is substantially weaker ($m_{obs}\approx -48\pm 7$ MHz cm). We note that satisfactory agreement between observed and predicted values of temporally averaged frequency shifts was obtained by Smith and co-workers [22], using a similar PW-OPO-LP model [21,22].

For modest values of $|\Delta k|$ (less than ~ 0.9 cm^{-1}), predictions of the PW-OPO-BB model (not shown in Fig. 5) agree well with those of the monochromatic PW-OPO-LP model. However, for values of $|\Delta k|$ above ~ 0.9 cm^{-1}, we find that the $f_{inst}(t)$ curve predicted by PW-OPO-BB starts to deviate from that of PW-OPO-LP in the central part of the pulse. This is attributable to breakdown in backconversion and corresponding increase in optical bandwidth, as discussed in Subsection 3.A; the pump threshold for this breakdown is reduced in the presence of nonzero Δk, as is further explored in Subsection 3.C. The signal output pulse profiles in the left-hand column of Fig. 5 have a reduced duration as $|\Delta k|$ increases, owing to reduced gain—and therefore larger buildup time and earlier signal-pulse termination—in the presence of phase mismatch.

It should be noted that conversion of signal and idler radiation back into pump radiation has long been recognized as a significant element in the above-threshold operation of nanosecond-pulsed OPOs [5,22–28]. For instance, such backconversion effects were identified in early experiments by modeling temporal profiles for OPO pump-wave depletion [22,27], by observing other characteristics such as output-beam quality and spectral properties [22], and via sidebands in the signal output from a pulsed OPO that is injection-seeded at two distinct idler wavelengths [28].

C. Optical Bandwidth, Partial Seeding, and Spectral Purity

As discussed in Subsections 3.A and 3.B, a reduction of backconversion in certain circumstances is accompanied by a significant increase of optical bandwidth, and by fast modulation (on a picosecond time scale) in the amplitude during the development of the signal and idler pulses [5,9,18], so that injection seeding breaks down during the pulse generation. Under typical operating conditions—with injection seeding, exact phase matching, and a pump pulse energy E_p of less than three times the unseeded threshold ($R_p<3$)—the OPO operates below the breakpoint for backconversion and injection seeding. Therefore, we seldom observe a breakdown in backconversion and injection seeding while the OPO is operating optimally.

According to Smith's simulations (e.g., see Fig. 6 in [9]), the breakpoint for our PPKTP OPO is approximately five times the unseeded threshold: close to the damage threshold of the PPKTP crystal. Given that our main goal is to have a FT-limited narrowband coherent light source for high-resolution spectroscopy [10,11], OPO operation is typically maintained below the breakpoint. However, when $|\Delta k|$ is large (e.g., above 0.5 cm^{-1}), a breakdown in narrowband seeded operation is often observed at lower pump-pulse energy ($R_p=\sim 3$) and the signal output pulse then undergoes a transition from SLM to multimode operation, as previously reported [3,4].

The OH detection system provides useful information on the evolution of the OPO output's spectral purity, which we define as the fraction of the pulse energy contained in the seeded longitudinal mode of the OPO cavity. For example, as the signal pulse evolves from SLM to multimode operation, the modulation depth of the OH beats decreases as the pulse becomes more broadband [3,4]. However, the OH detection system, with its limited bandwidth, cannot yield complete information on the temporal evolution of the optical spectrum of the pulse. In the absence of observed spectrotemporal data, numerical models (such as SNLO) can provide distinctive insight. Our earlier experiments [4] demonstrated the transition from seeded to partially seeded operation of the OPO (operating with significant phase mismatch) as R_p was increased from 1.6 to 3.5. During those measurements, the seeded signal wavelength ($\lambda_s=841.78$ nm) was offset from the free-running wavelength ($\lambda_{free}=841.94$ nm), such that $\Delta k=-0.69$ cm^{-1}.

Figure 6 shows the results of corresponding PW-OPO-BB simulations for five values of R_p, as follows: (a)–(c) 1.6; (d)–(f) 2.0; (g)–(i) 2.5; (j)–(l) 3.0; and (m)–(o) 3.5. The results for the OPO signal output are arranged in three columns for easy cross reference: simulated and measured pulse temporal profiles, including rapid walk-off oscillations in the simulations, in the left-hand column [(a), (d), (g), (j), (m)]; simulated and experimental instantaneous-frequency profiles in the central column [(b), (e), (h), (k), (n)]; optical bandwidth and spectral purity (each simulated by the PW-OPO-BB model) in the right-hand column [(c), (f), (i), (l), (o)]. The smoothed simulated pulse profiles and instantaneous-frequency profiles are generated with a 1 GHz numerical spectral filter to simulate the frequency response of our OH detection system. The transition to multimode operation is evident in the simulated output signal pulse profiles in the left-hand column of Fig. 6, with characteristic high-frequency amplitude oscillations that are attributable [9] to the estimated signal–idler walk-off of ~ 3 ps, together with an associated increase in power.

The evolution of the optical bandwidth $\Delta\nu$ of the signal radiation is shown, with left-hand ordinate, in the right-hand column of Fig. 6. Each of these curves was calculated by separating the complex-valued signal field profile into 1 ns sections and Fourier transforming each section (with 1 GHz resolution). Figure 7 shows optical spectra for two 1 ns sections of the OPO output signal pulse, with $R_p=3.5$ and $\Delta k=-0.69$ cm^{-1}. These correspond to the bottom row of plots (m), (n), and (o) in Fig. 6, for two different time intervals, namely: $t_1=15-16$ ns and $t_2=28-29$ ns, as

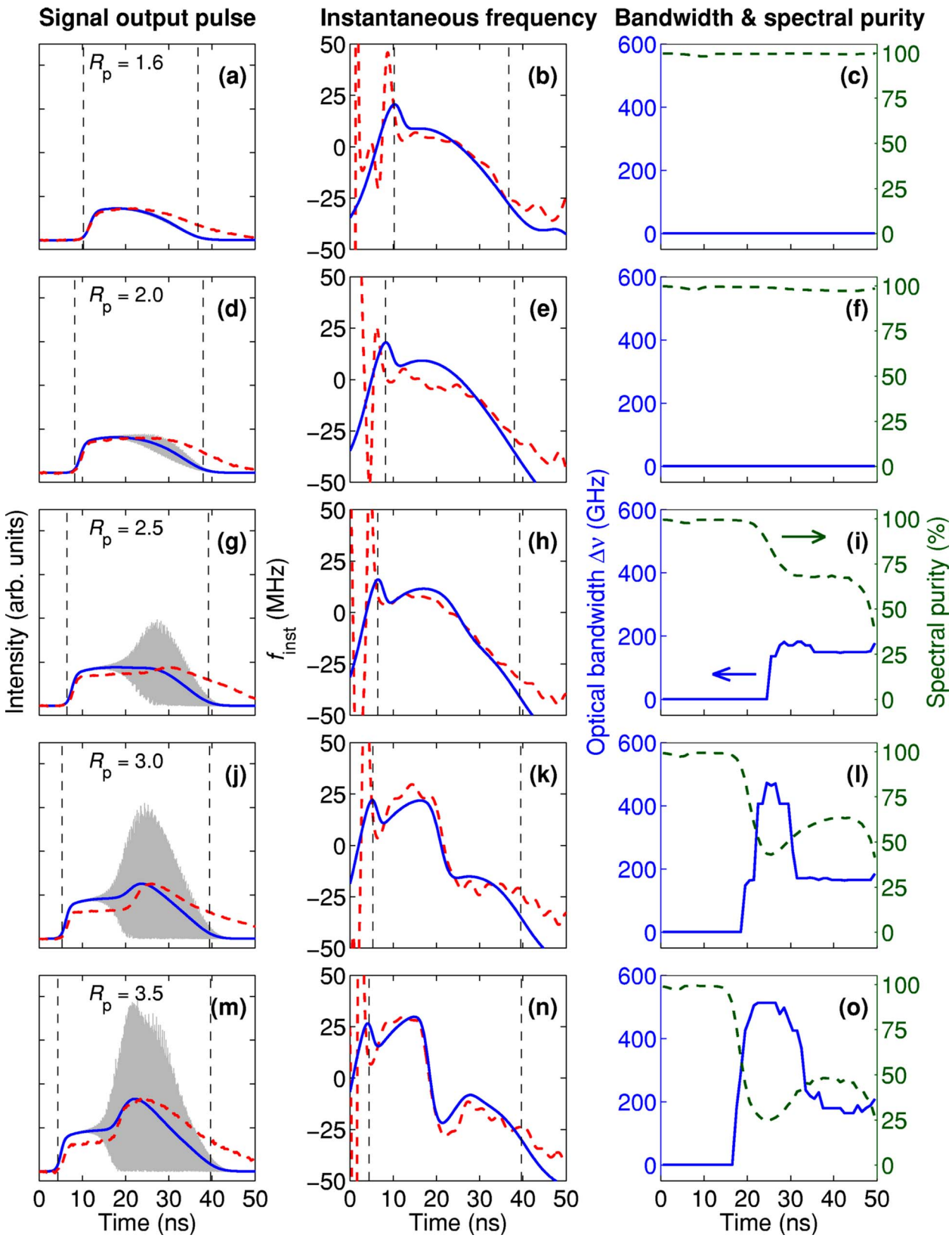

Fig. 6. (Color online) SNLO PW-OPO-BB simulations [17] of signal output pulses from an injection-seeded PPKTP OPO as in previous experiments [4] with $\lambda_s = 841.78$ nm and $\lambda_{free} = 841.94$ nm, resulting in a large phase mismatch ($\Delta k = -0.69\ \mathrm{cm}^{-1}$) that yields a transition from SLM to multimode operation as the times-above-threshold parameter R_p increases over a range from $R_p = 1.6$ [(a)–(c)] to $R_p = 3.5$ [(m)–(o)]. The left-hand column [(a), (d), (g), (j), (m)] depicts simulated and measured temporal profiles, including rapid walk-off oscillations in the simulations. The central column [(b), (e), (h), (k), (n)] depicts simulated and experimental profiles of the instantaneous frequency $f_{inst}(t)$. The right-hand column [(c), (f), (i), (l), (o)] depicts the optical bandwidth $\Delta\nu$ (left-hand ordinate) and the spectral purity (right-hand ordinate), each simulated by the PW-OPO-BB model.

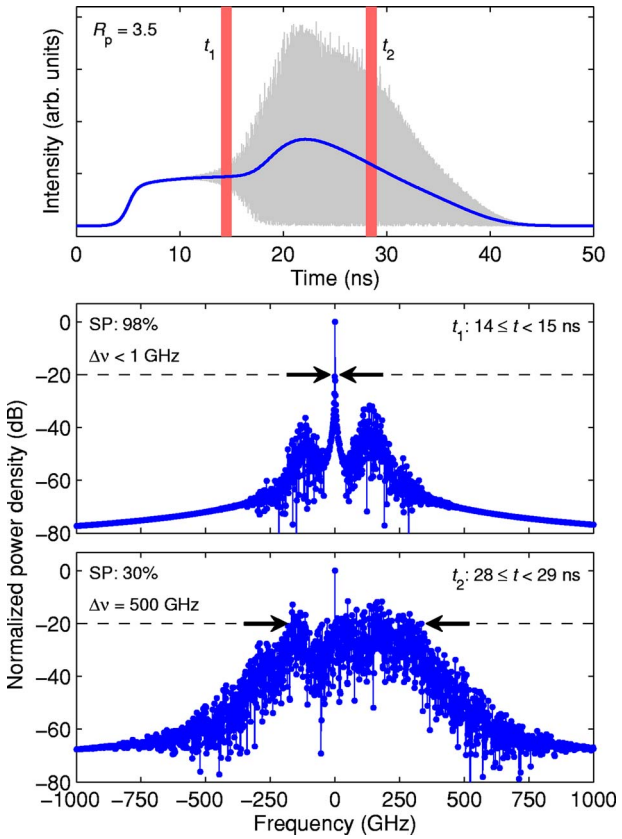

Fig. 7. (Color online) Top: PW-OPO-BB simulation of signal intensity for the OPO pulse output with $R_p=3.5$ and $\Delta k=-0.69\ \mathrm{cm}^{-1}$ as in Fig. 6(m), indicating two 1 ns time intervals ($t_1=15-16$ ns and $t_2=28-29$ ns) that are used for Fourier transformation to generate the spectra shown in the lower panels. Center: normalized power-density spectrum (after Fourier transformation of the complex-valued signal amplitude) for time interval t_1, yielding a narrow optical bandwidth $\Delta\nu$ (above the −20 dB level) and a high spectral purity (SP). Bottom: corresponding spectrum for time interval t_2, yielding a much broader optical bandwidth $\Delta\nu$ (~500 GHz above the −20 dB level) and a spectral purity of 30%, with a much less prominent central SLM peak. These spectra correlate with the results plotted in Fig. 6(o).

indicated in the top panel of Fig. 7. Here, the optical bandwidth parameter $\Delta\nu$ is arbitrarily defined as the frequency span between the highest and lowest frequency components with power levels of >1% of the maximum-power component (i.e., above −20 dB, as indicated by the dashed lines and horizontal arrows in the lower two panels of Fig. 7).

With a pump pulse energy equivalent to $R_p=3.5$ and phase mismatch $\Delta k=-0.69\ \mathrm{cm}^{-1}$, the time interval $t_1=15-16$ ns occurs during the onset of injection-seeding breakdown in the OPO. The central panel of Fig. 7 therefore shows that a strong central (SLM) peak is the only feature exceeding the −20 dB level, so that $\Delta\nu$ is small (<1 GHz). By contrast, the breakdown of injection seeding is pronounced in the bottom panel of Fig. 7, which corresponds to the time interval $t_2=28-29$ ns and yields a much larger bandwidth ($\Delta\nu=500$ GHz), in view of the wide spread of Fourier components exceeding the −20 dB level. Figure 6 shows that, if $R_p\geq 2$, the bandwidth is initially low (less than the 1 GHz limit of fast FT resolution), indicating that seeding is effective early in the pulse (as in the central panel of Fig. 7) but that it increases significantly (to several hundred gigahertz) from ~20 ns onward (as in the bottom panel of Fig. 7).

Also shown in the right-hand column of Fig. 6, with right-hand ordinate, is the spectral purity, which is defined here as the fraction of the signal output pulse energy that lies within 1 GHz of the seeded mode; it decreases significantly as seeding fails (from an initial value of 100% to a minimum of 25% at 25 ns when $R_p=3.5$). As the broadband component is centered away from the seeded mode, the spectral purity provides a measure of the fractional power in the seeded mode. In the examples shown in Fig. 7, the values of spectral purity are 98% and 30% for time intervals t_1 (central panel) and t_2 (bottom panel), respectively.

The results in Fig. 6 show that, when $R_p<2$, the OPO is effectively seeded with narrow optical bandwidth and spectral purity of >97% throughout the pulse; despite the presence of large phase mismatch ($\Delta k=-0.69\ \mathrm{cm}^{-1}$). Additional simulations show that the sign of Δk is responsible for asymmetry that occurs in spectra such as that in the bottom trace of Fig. 7 where negative Δk causes the spectrum to be more prominent on the high-frequency side of the SLM peak; in contrast positive Δk tends to displace the more prominent wing of the spectrum onto the low-frequency side of the SLM peak.

It is interesting to compare the simulated and experimental $f_{\mathrm{inst}}(t)$ curves presented for the partially seeded OPO in the central column of Fig. 6. These can be correlated with the results in the adjacent columns of Fig. 6. The negative value of Δk produces negative overall frequency chirp (approximately −50 MHz for $R_p=2$), which is approximately linear at low pump levels ($R_p<2.5$) but becomes modulated at large pump levels ($R_p>2.5$). This effect appears to be predictable, as the simulations are in highly satisfactory agreement with our observations.

4. CONCLUSIONS

The performance of a nanosecond-pulsed, injection-seeded OPO based on PPKTP has been numerically simulated by using plane-wave (PW) approximations that are available in the SNLO nonlinear-optical software package [17]. This approach provides insight into complicated spectrotemporal dynamics during OPO signal and idler pulse generation. Our work is guided by recent studies of optical bandwidth and group-velocity effects in nanosecond-pulsed OPOs [5,9]. The outcome of our simulations agrees well with our previously reported experimental results [3,4]. We are particularly satisfied that simulated profiles of the instantaneous frequency $f_{\mathrm{inst}}(t)$ match experimental results for a range of values of phase mismatch Δk and pump pulse energy E_p [3]. The resulting simulations of spectrotemporal characteristics, many of which are presented for the first time to the best of our knowledge, are especially useful in providing insight into aspects of the performance of a pulsed OPO that are not readily determined by experiment. For example, they allow us to estimate the evolution of the optical bandwidth and spectral purity of the output signal and idler pulses and also to recognize the occurrence of rapid walk-off oscillations that are associated with a breakdown in backconversion

and injection seeding owing to group-velocity mismatch [5,9]. These oscillations, which are too rapid to observe with the photodetectors regularly used in our optical-heterodyne (OH) detection system, indicate a partial failure of injection seeding and a transition from SLM to multimode operation as previously observed [3,4]. Our simulations explore instrumental conditions that facilitate continuously tunable SLM operation of such a pulsed OPO system, with optical bandwidth as close as possible to the Fourier-transform (FT) limit. The excellent agreement between the simulations and experiment encourages us to be confident that our injection-seeded OPO is a well-characterized, reliable source of tunable, narrowband, coherent radiation for high-resolution spectroscopy on a nanosecond timescale.

ACKNOWLEDGMENTS

We acknowledge financial support from the Australian Research Council. We appreciate helpful communications with Arlee Smith.

REFERENCES

1. R. T. White, Y. He, B. J. Orr, M. Kono, and K. G. H. Baldwin, "Pulsed injection-seeded optical parametric oscillator with low frequency chirp for high-resolution spectroscopy," Opt. Lett. **28**, 1248–1250 (2003).
2. R. T. White, Y. He, B. J. Orr, M. Kono, and K. G. H. Baldwin, "Control of frequency chirp in nanosecond-pulsed laser spectroscopy. 1. Optical-heterodyne chirp analysis techniques," J. Opt. Soc. Am. B **21**, 1577–1585 (2004).
3. R. T. White, Y. He, B. J. Orr, M. Kono, and K. G. H. Baldwin, "Control of frequency chirp in nanosecond-pulsed laser spectroscopy. 2. A long-pulse optical parametric oscillator for narrow optical bandwidth," J. Opt. Soc. Am. B **21**, 1586–1594 (2004).
4. R. T. White, Y. He, B. J. Orr, M. Kono, and K. G. H. Baldwin, "Transition from single-mode to multimode operation of an injection-seeded pulsed optical parametric oscillator," Opt. Express **12**, 5655–5660 (2004).
5. G. Arisholm, G. Rustad, and K. Stenersen, "Importance of pump-beam group velocity for backconversion in optical parametric oscillators," J. Opt. Soc. Am. B **18**, 1882–1890 (2001).
6. G. Anstett, A. Borsutzky, and R. Wallenstein, "Investigation of the spatial beam quality of pulsed ns-OPOs," Appl. Phys. B **76**, 541–545 (2003).
7. G. Anstett, M. Nitmann, and R. Wallenstein, "Experimental investigation and numerical simulation of the spatio-temporal dynamics of the light pulses in nanosecond optical parametric oscillators," Appl. Phys. B **79**, 305–313 (2004).
8. G. Anstett and R. Wallenstein, "Experimental investigation of the spectro-temporal dynamics of the light pulses of *Q*-switched Nd:YAG lasers and nanosecond optical parametric oscillators," Appl. Phys. B **79**, 827–836 (2004).
9. A. V. Smith, "Bandwidth and group-velocity effects in nanosecond optical parametric amplifiers and oscillators," J. Opt. Soc. Am. B **22**, 1953–1965 (2005).
10. M. Kono, K. G. H. Baldwin, R. T. White, Y. He, and B. J. Orr, "Heterodyne-assisted pulsed spectroscopy with a nearly Fourier-transform limited, injection-seeded optical parametric oscillator," Opt. Lett. **30**, 3413–3415 (2005).
11. M. Kono, K. G. H. Baldwin, R. T. White, Y. He, and B. J. Orr, "CHAPS: a new precision laser-spectroscopic technique," J. Opt. Soc. Am. B **23**, 1181–1189 (2006).
12. R. T. White, "Quasi-phase-matched nonlinear-optical devices," Ph.D. dissertation (Macquarie University, Sydney, 2004).
13. F. J. Harris, "On the use of windows for harmonic analysis with the discrete Fourier transform," Proc. IEEE **66**, 51–83 (1978).
14. S. Gangopadhyay, N. Melikechi, and E. E. Eyler, "Optical phase perturbations in nanosecond pulsed amplification and second-harmonic generation," J. Opt. Soc. Am. B **11**, 231–241 (1994).
15. N. Melikechi, S. Gangopadhyay, and E. E. Eyler, "Phase dynamics in nanosecond pulsed dye laser amplification," J. Opt. Soc. Am. B **11**, 2402–2411 (1994).
16. S. Gangopadhyay, "Optical phase distortions in nanosecond laser pulses and their effects on high resolution spectroscopy," Ph.D. dissertation (University of Delaware, 1995).
17. A. V. Smith, SNLO, public-domain software (Sandia National Laboratories). It is available as a free download at http://www.sandia.gov/imrl/X1118/xxtal.htm.
18. A. V. Smith, R. J. Gehr, and M. S. Bowers, "Numerical models of broad-bandwidth nanosecond optical parametric oscillators," J. Opt. Soc. Am. B **16**, 609–619 (1999).
19. E. S. Cassedy and M. Jain, "A theoretical study of injection tuning of optical parametric oscillators," IEEE J. Quantum Electron. **QE-15**, 1290–1301 (1979).
20. K. Kato and E. Takaoka, "Sellmeier and thermo-optic dispersion formulas for KTP," Appl. Opt. **41**, 5040–5044 (2002).
21. T. D. Raymond, W. J. Alford, A. V. Smith, and M. S. Bowers, "Frequency shifts in injection-seeded optical parametric oscillators with phase mismatch," Opt. Lett. **19**, 1520–1522 (1994).
22. A. V. Smith, W. J. Alford, T. D. Raymond, and M. S. Bowers, "Comparison of a numerical model with measured performance of a seeded, nanosecond KTP optical parametric oscillator," J. Opt. Soc. Am. B **12**, 2253–2267 (1995).
23. S. E. Harris, "Tunable optical parametric oscillators," Proc. IEEE **57**, 2096–2113 (1969).
24. J. E. Bjorkholm, "Some effects of spatially nonuniform pumping in pulsed optical parametric oscillators," IEEE J. Quantum Electron. **QE-7**, 109–118 (1971).
25. R. A. Baumgartner and R. L. Byer, "Optical parametric amplification," IEEE J. Quantum Electron. **QE-15**, 432–444 (1979).
26. Y. X. Fan, R. C. Eckardt, R. L. Byer, J. Nolting, and R. Wallenstein, "Visible BaB_2O_4 optical parametric oscillator pumped by a single-axial-mode pulsed source," Appl. Phys. Lett. **53**, 2014–2016 (1988).
27. M. J. Johnson, "Development of pulsed, tunable, optical parametric oscillators for spectroscopic applications," Ph.D. dissertation (Macquarie University, 1995).
28. G. W. Baxter, J. G. Haub, and B. J. Orr, "Backconversion in a pulsed optical parametric oscillator: evidence from injection-seeded sidebands," J. Opt. Soc. Am. B **14**, 2723–2730 (1997).